

Electrochemical hydrogen storage characteristics of as-cast and annealed $\text{La}_{0.8-x}\text{Nd}_x\text{Mg}_{0.2}\text{Ni}_{3.15}\text{Co}_{0.2}\text{Al}_{0.1}\text{Si}_{0.05}$ ($x=0-0.4$) alloys

Yang-huan ZHANG^{1,2}, Zhong-hui HOU², Bao-wei LI², Hui-ping REN², Ying CAI², Dong-liang ZHAO¹

1. Department of Functional Material Research, Central Iron and Steel Research Institute, Beijing 100081, China;

2. Elected State Key Laboratory, Inner Mongolia University of Science and Technology, Baotou 014010, China

Received 23 February 2012; accepted 10 April 2012

Abstract: The La–Mg–Ni-based A_2B_7 -type $\text{La}_{0.8-x}\text{Nd}_x\text{Mg}_{0.2}\text{Ni}_{3.15}\text{Co}_{0.2}\text{Al}_{0.15}$ ($x=0, 0.1, 0.2, 0.3, 0.4$) electrode alloys were prepared by casting and annealing. The influences of partial substitution of Nd for La on the structure and electrochemical performance of the as-cast and annealed alloys were investigated. It was found that the experimental alloys consist of two major phases, $(\text{La}, \text{Mg})_2\text{Ni}_7$ phase with the hexagonal Ce_2Ni_7 -type structure and LaNi_5 phase with the hexagonal CaCu_5 -type structure, as well as some residual phase LaNi_3 and NdNi_5 . The discharge capacity and high rate discharge ability (HRD) of the as-cast and annealed alloys first increase and then decrease with Nd content growing. The as-cast and annealed alloys ($x=0.3$) yield the largest discharge capacities of 380.3 and 384.3 mA·h/g, respectively. The electrochemical cycle stability of the as-cast and annealed alloys markedly grows with Nd content rising. As the Nd content increase from 0 to 0.4. The capacity retaining rate (S_{100}) at the 100th charging and discharging cycle increases from 64.98% to 85.17% for the as-cast alloy, and from 76.60% to 96.84% for the as-annealed alloy.

Key words: Ni–MH battery; hydrogen storage; A_2B_7 -type electrode alloy; Nd; La; substitution; electrochemical characteristics

1 Introduction

Since KADIR et al [1] and KOHNO et al [2] reported their research results, RE–Mg–Ni-system AB_3 - and A_2B_7 -type alloys have attracted considerable attention in the light of their high hydrogen storage capacity, good electrode properties and low production costs [3–5]. The investigation on the structure and electrochemical properties of the alloys has made great progress, about which LIU et al gave a perfect summarization recently [6]. However, the production of the new-type alloys as the negative electrode in Ni–MH battery has not been found in China on account of little poor electrochemical cycle stability of the electrode alloys. Hence, it is still one of the major challenges faced by researchers in this area to find ways to improve the cycle stability and maintaining its discharge capacity.

It has come to light that the capacity deterioration of the La–Mg–Ni system alloy electrodes is mainly associated with the pulverization of the alloy particles

and the oxidation/corrosion of the elements Mg and La during electrochemical charge–discharge cycling [7,8]. Furthermore, element substitution, in general, is an effective method for improving the overall electrode properties of the hydrogen-storage alloys. In the case of La–Mg–Ni series hydrogen-storage alloys, the partial replacement of Ni with Co, Fe, Mn, Al, Cu [9,10] and of La with Ce, Pr, Nd [11–13] were studied systematically.

In this work, it is expected that a combination of decreasing Mg content and substituting La with Nd will improve the electrochemical cycle stability of the La–Mg–Ni system A_2B_7 -type alloys. Hence, a systematic investigation about the effects of the substitution of Nd for La and annealing treatment on the structures and electrochemical properties of the $\text{La}_{0.8-x}\text{Nd}_x\text{Mg}_{0.2}\text{Ni}_{3.15}\text{Co}_{0.2}\text{Al}_{0.15}$ ($x=0-0.4$) electrode alloys has been performed.

2 Experimental

The compositions of the prepared alloys were

Foundation item: Projects (51161015, 50961009) supported by the National Natural Science Foundations of China; Project (2011AA03A408) supported by the National Hi-tech Research and Development Program of China; Projects (2011ZD10, 2010ZD05) supported by the Natural Science Foundation of Inner Mongolia, China

Corresponding author: Yang-huan ZHANG; Tel: +86-10-62183115; E-mail: zyh59@yahoo.com.cn
DOI: 10.1016/S1003-6326(13)62610-2

$\text{La}_{0.8-x}\text{Nd}_x\text{Mg}_{0.2}\text{Ni}_{3.15}\text{Co}_{0.2}\text{Al}_{0.1}\text{Si}_{0.05}$ ($x=0, 0.1, 0.2, 0.3, 0.4$). For convenience, the alloys were denoted with Nd content as $\text{Nd}_0, \text{Nd}_{0.1}, \text{Nd}_{0.2}, \text{Nd}_{0.3}$ and $\text{Nd}_{0.4}$, respectively. The alloy ingots were prepared using a vacuum induction furnace. A part of the alloy was annealed at 950 °C for 8 h. Before annealing, the as-cast samples were first sealed in a quartzes glass tube filled with helium, and then it was put into a vacuum tube furnace for annealing. The melting and annealing were performed in helium atmosphere under a pressure of 0.04 MPa for the sake of preventing the volatilization of Mg.

The phase structures and compositions of the alloys were determined by XRD (Dmax/2400). The diffraction with the experimental parameters of 160 mA, 40 kV and 10(°)/min, was performed with Cu $K_{\alpha 1}$ radiation filtered by graphite. A Philips SEM (QUANTA 400) linked with an energy dispersive spectrometer (EDS) was used for morphological characterization and chemical analysis of the as-cast and annealed alloys.

Round electrode pellets with a diameter of 15 mm were obtained by cold pressing a mixture of the alloy powder and carbonyl nickel powder in the mass ratio of 1:4 under a pressure of 35 MPa. After being dried for 4 h, the electrode pellets were immersed in a 6 mol/L KOH solution for 24 h in order to fully wet the electrodes before the electrochemical measurements.

The electrochemical measurements were performed at 30 °C with a tri-electrode open cell, consisting of a working electrode (the metal hydride electrode), a sintered $\text{Ni}(\text{OH})_2/\text{NiOOH}$ counter electrode and a Hg/HgO reference electrode, which were immersed in a 6 mol/L KOH electrolyte. The voltage between the negative electrode and the reference electrode was defined as the discharge voltage. In every cycle, the alloy electrode was first charged with a constant current density, followed by the resting for 15 min, then it was discharged at the same current density to a cut-off voltage of -0.5 V.

The electrochemical impedance spectra (EIS) and the Tafel polarization curves of the alloys were measured using an electrochemical workstation (PARSTAT 2273). The fresh electrodes were fully charged and then rested for 2 h up to the stabilization of the open circuit potential. The EIS of the alloy electrodes were measured in the frequency ranging from 10 kHz to 5 mHz at 50% depth of discharge (DOD). The Tafel polarization curves were measured in the potential range of -1.2 to +1.0 V (vs Hg/HgO) with a scanning rate of 5 mV/s. For the potentiostatic discharge, the test electrodes in the fully charged state were discharged at 500 mV potential step for 5000 s at the electrochemical workstation (PARSTAT 2273), using the electrochemistry corrosion software (CorrWare).

3 Results and discussion

3.1 Structural characteristics

Figure 1 depicts the XRD patterns of the as-cast and annealed $\text{La}_{0.8-x}\text{Nd}_x\text{Mg}_{0.2}\text{Ni}_{3.15}\text{Co}_{0.2}\text{Al}_{0.1}\text{Si}_{0.05}$ ($x=0-0.4$) alloys. All the as-cast and annealed alloys hold a multiphase structure consisting of two major phases ($\text{La,Mg})_2\text{Ni}_7$ and LaNi_5 as well as some residual phase LaNi_3 and NdNi_5 . The substitution of Nd for La brings on forming NdNi_5 phase in the as-cast and annealed alloys without changing their two major phases. The lattice parameters and the phase abundances of the two major phases, $(\text{La,Mg})_2\text{Ni}_7$ and LaNi_5 , in the as-cast and annealed alloys, calculated from the XRD data by Jade 6.0 software, are listed in Table 1. It shows that the substitution of Nd for La notably reduces the lattice constants and cell volumes of two major phases $(\text{La,Mg})_2\text{Ni}_7$ and LaNi_5 in the alloys, due to the smaller atom radius of Nd than that of La. The reduction of the cell volume, caused by the Nd substitution, justifies the successful alloying of Nd with two major phases. Furthermore, such substitution incurs a decrease in the $(\text{La,Mg})_2\text{Ni}_7$ phase and an increase in the LaNi_5 phase.

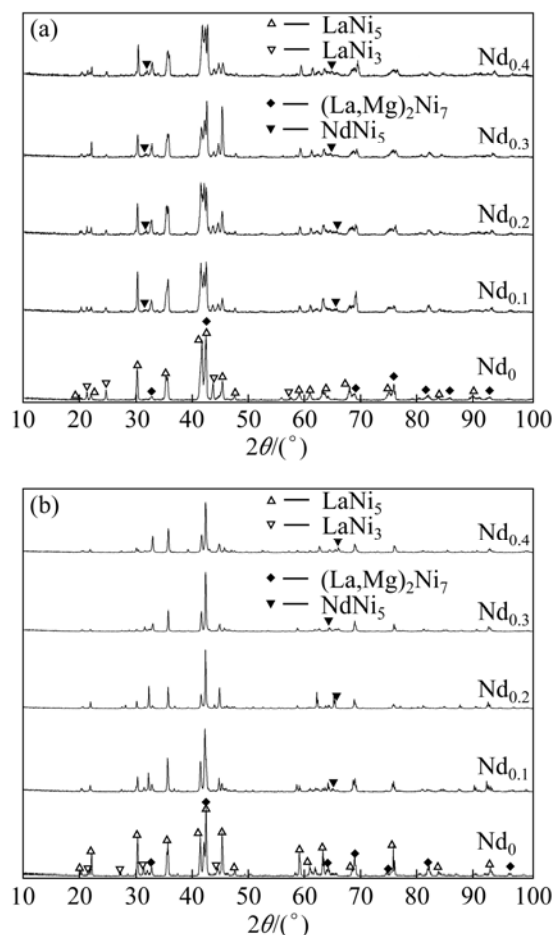


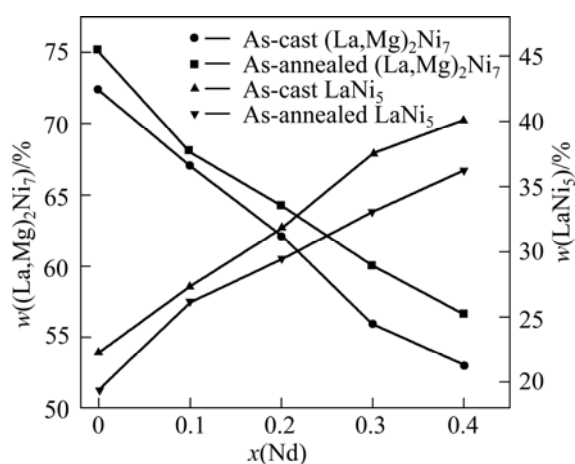
Fig. 1 XRD patterns of as-cast (a) and annealed (b) alloys

Table 1 Lattice constants and abundances of LaNi₅ and (La,Mg)₂Ni₇ phases

State	Alloy	Major phase	Lattice constant		Cell volume/nm ³	Phase abundance in mass fraction/%	
			a/nm	c/nm			
As-cast	Nd ₀	(La,Mg) ₂ Ni ₇	0.50648	2.46521	0.5476	72.32	
		LaNi ₅	0.50573	0.41289	0.0915	22.28	
	Nd _{0.1}	(La,Mg) ₂ Ni ₇	0.50502	2.45874	0.5431	67.05	
		LaNi ₅	0.50518	0.41165	0.0910	27.25	
	Nd _{0.2}	(La,Mg) ₂ Ni ₇	0.50467	2.45116	0.5406	62.13	
		LaNi ₅	0.50411	0.41013	0.0903	31.77	
	Nd _{0.3}	(La,Mg) ₂ Ni ₇	0.50381	2.44012	0.5364	55.89	
		LaNi ₅	0.50312	0.40677	0.0892	37.51	
	Nd _{0.4}	(La,Mg) ₂ Ni ₇	0.50259	2.43152	0.5319	53.02	
		LaNi ₅	0.50169	0.40214	0.0877	40.08	
	As-annealed	Nd ₀	(La,Mg) ₂ Ni ₇	0.50689	2.46709	0.5489	75.01
			LaNi ₅	0.50581	0.41279	0.0915	19.39
Nd _{0.1}		(La,Mg) ₂ Ni ₇	0.50609	2.46012	0.5457	68.02	
		LaNi ₅	0.50553	0.41185	0.0911	26.18	
Nd _{0.2}		(La,Mg) ₂ Ni ₇	0.50511	2.45603	0.5427	64.22	
		LaNi ₅	0.50503	0.41049	0.0907	29.48	
Nd _{0.3}		(La,Mg) ₂ Ni ₇	0.50422	2.44878	0.5391	60.02	
		LaNi ₅	0.50404	0.40745	0.0896	33.08	
Nd _{0.4}		(La,Mg) ₂ Ni ₇	0.50321	2.44071	0.5352	56.69	
		LaNi ₅	0.50215	0.40303	0.0880	36.21	

A very similar result has been reported by CHEN et al [13,14]. It is quite evident that the width of the diffraction peaks of the (La,Mg)₂Ni₇ phase and LaNi₅ phase becomes markedly narrow after annealing treatment, indicating that the annealing treatment renders the composition homogenization of the alloys [15]. In order to observe the Nd content dependence of the abundances of the major phases in the alloys, the evolution of the abundances of two major phases (La,Mg)₂Ni₇ and LaNi₅ in the as-cast and annealed alloys with the amount of Nd substitution is shown in Fig. 2. For the same Nd content, the annealing treatment leads to an evident increase in the (La,Mg)₂Ni₇ phase and a decrease in the LaNi₅ phase.

Figure 3 shows the SEM images and EDS spectra of the as-cast and annealed Nd₀ and Nd_{0.4} alloys. It is evident that the as-cast alloys display a dendrite structure. The substitution of Nd for La brings on a notable refinement of the grains of the as-cast and annealed alloys. The annealing treatment obviously improves the segregation of the composition in the alloys. The EDS analysis shows that all the experimental alloys hold a multiphase structure, consisting of (La,Mg)₂Ni₇ (denoted

**Fig. 2** Evolution of abundances of major phases LaNi₅ and (La,Mg)₂Ni₇ with Nd content (x)

as A) and LaNi₅ (denoted as B) as well as LaNi₃ (denoted as C) phases, which conforms well to the XRD observation. Because the amount of NdNi₅ phase is small and it attaches itself to (La,Mg)₂Ni₇ or LaNi₅ phase in the process of growing, it is difficult to observe its morphology.

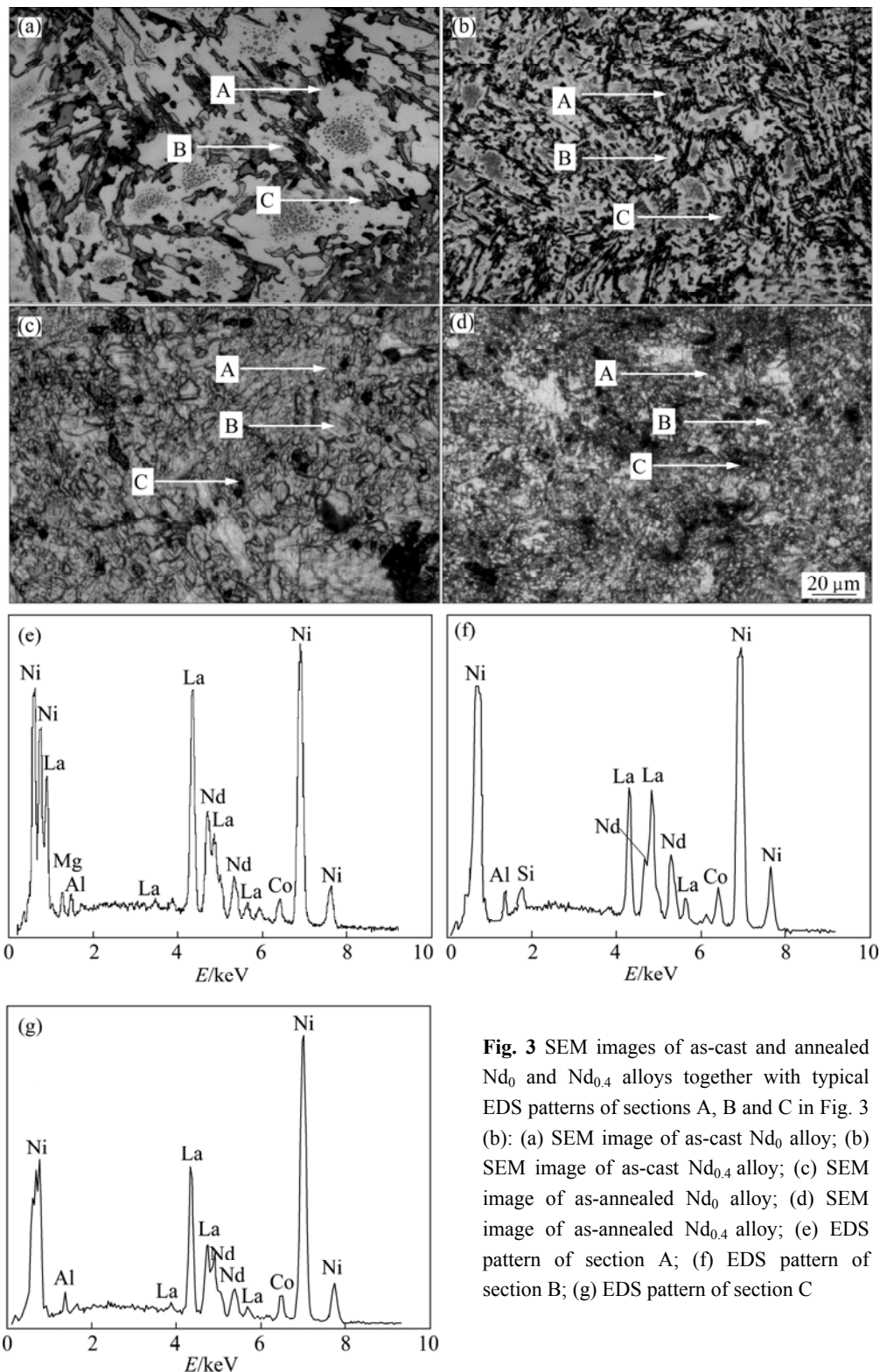


Fig. 3 SEM images of as-cast and annealed Nd_0 and $\text{Nd}_{0.4}$ alloys together with typical EDS patterns of sections A, B and C in Fig. 3 (b): (a) SEM image of as-cast Nd_0 alloy; (b) SEM image of as-cast $\text{Nd}_{0.4}$ alloy; (c) SEM image of as-annealed Nd_0 alloy; (d) SEM image of as-annealed $\text{Nd}_{0.4}$ alloy; (e) EDS pattern of section A; (f) EDS pattern of section B; (g) EDS pattern of section C

3.2 Electrochemical performance

3.2.1 Electrochemical cycle stability

The electrochemical cycle stability of the alloy electrode, an essential factor determining the life span of the Ni–MH battery, is signified by the capacity retaining rate (S_n), defined as $S_n = C_n / C_{\max} \times 100\%$, where C_{\max} is the

maximum discharge capacity and C_n is the discharge capacity of the n th charge–discharge cycle at a current density of 300 mA/g. Figure 4 shows the evolution of the capacity retaining rate (S_n) of the as-cast and annealed alloys with the cycle number n . The slopes of the curves in Fig. 4 indicate the degradation rate of

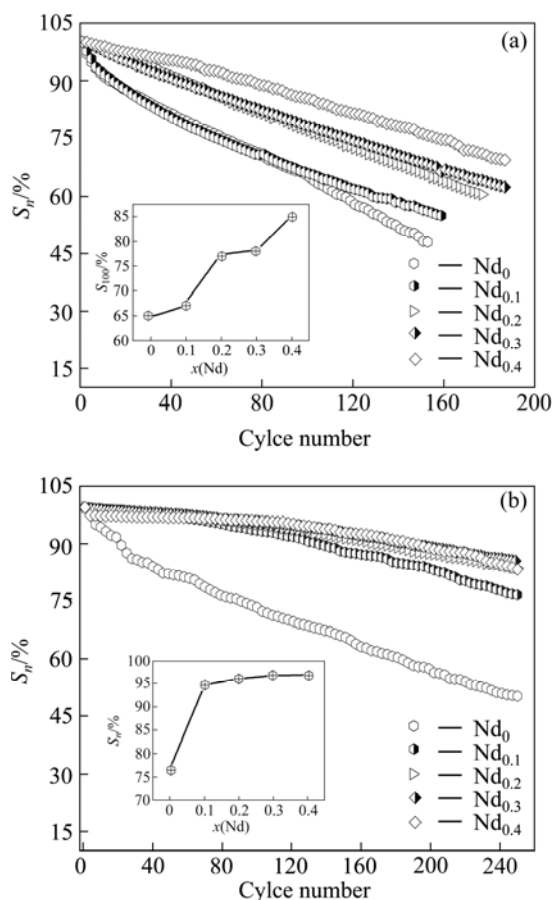


Fig. 4 Evolution of capacity retaining rates (S_n) of alloys with cycle number: (a) As-cast; (b) As-annealed

the discharge capacity in the charging–discharging cycle. The smaller the slope of the curve is, the better the cycle stability of the alloy will be. It can be seen that the change of the curve slopes of the as-cast alloys is unobvious with the variation of Nd content, whereas the slope of the curves of as-annealed alloys substituted by Nd is much smaller than that of the Nd-free alloy.

In order to observe the relationship between the capacity retaining rate and the Nd content, the amount of Nd substitution dependence of the capacity retaining rate (S_{100}) at the 100th charging–discharging cycle is also presented in Fig. 4. It indicates that the S_{100} values of the as-cast and annealed alloys markedly grow with increasing Nd content. The S_{100} value is enhanced from 64.98% to 85.17% for the as-cast alloy, and from 76.60% to 96.84% for the as-annealed alloy, by increasing Nd content from 0 to 0.4. It is derived by comparing Figs. 4 (a) with (b) that for the same Nd content, the as-annealed alloy exhibits much higher cycle stability than the as-cast one. It was well known that the lattice stress and the expansion of the cell volume, which are inevitable when hydrogen atoms enter into the interstitial sites of the lattice, are the real driving force that leads to the pulverization of the alloy. The positive impact of Nd

substitution on the cycle stability of the alloy is basically ascribed to two factors. Firstly, the refined grain by Nd substitution is instructive to enhancing the cycle stability on account of the anti-pulverization capability of the alloy basically depending on its grain size. Secondly, the increase of the LaNi_5 phase incurred by substituting La with Nd is beneficial to improving cycle stability of the alloys due to an unanswerable fact that LaNi_5 phase possesses a much higher electrochemical cycle stability than $(\text{La},\text{Mg})_2\text{Ni}_7$ phase. The benefaction of the annealing treatment on the cycle stability of the alloys is ascribed to the structure change and more homogeneous compositional distribution created by the annealing, which facilitates to prohibit the pulverization and corrosion of the alloy [15]. Our previous work has ascertained that the additive of a proper amount of Si can enhance the electrochemical cycle stability of the La–Mg–Ni-based A_2B_7 -type alloy considerably, which is probably ascribed to the improved anti-corrosion ability of the alloy by adding Si. The exact mechanism needs to be further investigated [16,17].

3.2.2 Activation capability and discharge capacity

The activation capability was indicated by the number of charging–discharging cycles required for attaining the greatest discharge capacity through the charging–discharging cycle at a constant current density of 60 mA/g. Figure 5 demonstrates the cycle number dependence of the discharge capacities of the as-cast and annealed alloys. It shows that all the alloys possess superior activation performance, attaining their maximum discharge capacities at two charging–discharging cycles. The excellent activation capability of the as-cast and annealed alloys is mainly ascribed to their multiphase structures because the phase boundary can decrease the lattice distortion and strain energy formed in the process of hydrogen absorption. Furthermore, the phase boundary provides good tunnels for diffusion of hydrogen atoms, improving the activation performance of the alloy. Figure 6 illustrates the Nd content dependence of the discharge capacity of the as-cast and annealed alloys at a charge–discharge current density of 60 mA/g. It displays that the discharge capacities of the as-cast and annealed alloys first mount up and then fall with Nd content growing. The as-cast and annealed alloys yield the largest discharge capacities of 380.2 and 384.0 mA·h/g respectively as Nd content is 0.3. It can be clearly seen from Fig. 6 that for the same Nd content, the as-annealed alloy exhibits a much higher discharge capacity than the as-cast one.

The discharge capacity of an alloy is dominated by multiple factors, one of which is the unit-cell volume due to the volume change of an alloy during hydriding proportional to the amount of hydrogen absorbed in cycling or the electrochemical capacity [18]. The

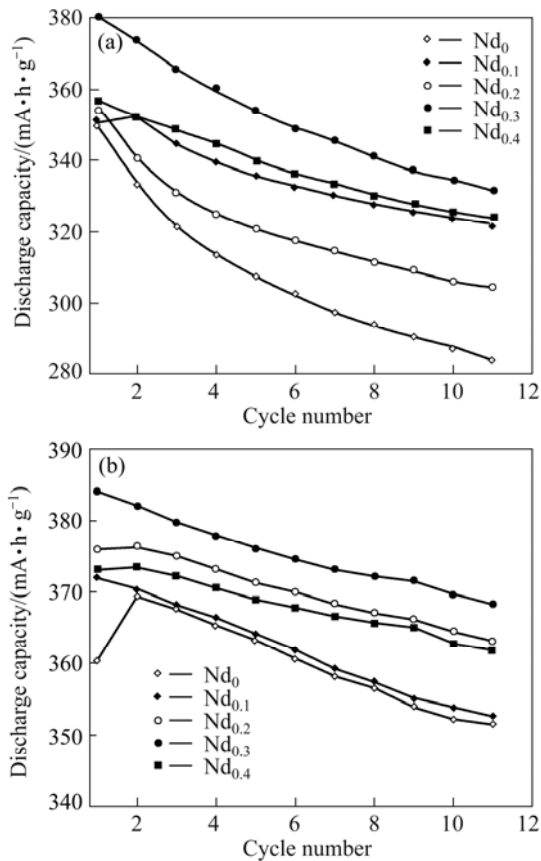


Fig. 5 Evolution of discharge capacity of alloys with cycle number: (a) As-cast; (b) As-annealed

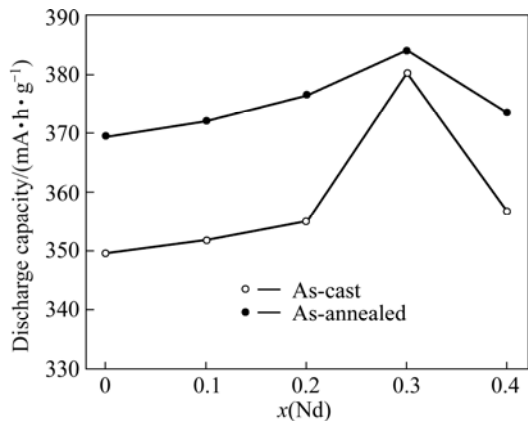


Fig. 6 Evolution of discharge capacity of as-cast and annealed alloys with Nd content

reduction of the cell volume and the $(\text{La,Mg})_2\text{Ni}_7$ phase originated from substituting La with Nd are evidently detrimental to the discharge capacity of the alloy. Therefore, it seems to be self-evident that such substitution turns out to be a decrease of the discharge capacities of the alloys. In fact, the as-cast and annealed alloys yield the maximum discharge capacities with the variation of Nd content, for which the changes of the phase abundances and structure of the alloys resulting from Nd substitution are basically responsible. The

refinement of the grain produced by Nd substitution is beneficial to the discharge capacity because the grain boundary exhibits the distribution of the maximum hydrogen concentrations [19]. Furthermore, it is noteworthy that the LaNi_5 phase works not only as a hydrogen reservoir but also as a catalyst to activate the $(\text{La,Mg})_2\text{Ni}_7$ phase to absorb/desorb hydrogen reversibly in the alkaline electrolyte [20]. The above contrary effects result in an optimum Nd content for the discharge capacity of the alloys. The annealing treatment notably enhances the discharge capacity of the alloy, attributed to the homogenization of the composition and the changes of the phase abundance and the lattice parameters originated from annealing treatment.

3.2.3 High rate discharge ability and electrochemical kinetics

The electrochemical hydrogen storage kinetics of the alloy electrode is characterized by its high rate discharge ability (HRD), calculated by the formula: $\text{HRD} = C_{J,\text{max}}/C_{60,\text{max}} \times 100\%$, where $C_{J,\text{max}}$ and $C_{60,\text{max}}$ are the maximum discharge capacities of the alloy electrode charged–discharged at current densities of J and 60 mA/g respectively. Figure 7 shows the relationship between the HRD values of the as-cast and annealed alloys and the discharge current density. It indicates that the HRD values of the as-cast and annealed alloys first augment then decline with Nd content growing. In order to demonstrate the influence of Nd content on the HRD values of the alloys, the Nd content dependence of the HRD values, for a fixed current density of 300 mA/g, of the as-cast and annealed alloys is also shown in Fig. 7. It is evident that the HRD value of the as-cast alloy is much higher than that of the as-annealed one for the same Nd content, suggesting that the annealing treatment impairs the high rate discharge ability of the alloys.

The high rate dischargeability of the metal hydride electrode is principally dominated by the charge-transfer rate on the alloy surface and the hydrogen diffusion capability in the alloy bulk. Hence, an investigation on the electrochemical kinetics of the alloys is quite necessary.

The hydrogen diffusion coefficients (D) of the as-cast and annealed alloys are measured by using a potential step technique. A potential step of +500 mV vs the stabilized open circuit potential of the fully charged electrode was applied and the change of the discharge current with time is recorded. Figure 8 demonstrates the semilogarithmic curves of anodic current vs working duration of the as-cast and annealed alloy electrodes. Based on the hydrogen diffusion model constituted by ZHENG et al [21], the diffusion coefficient of hydrogen atoms in the bulk of the alloy can be calculated through the slope of the linear region of the corresponding plots according to the formulae:

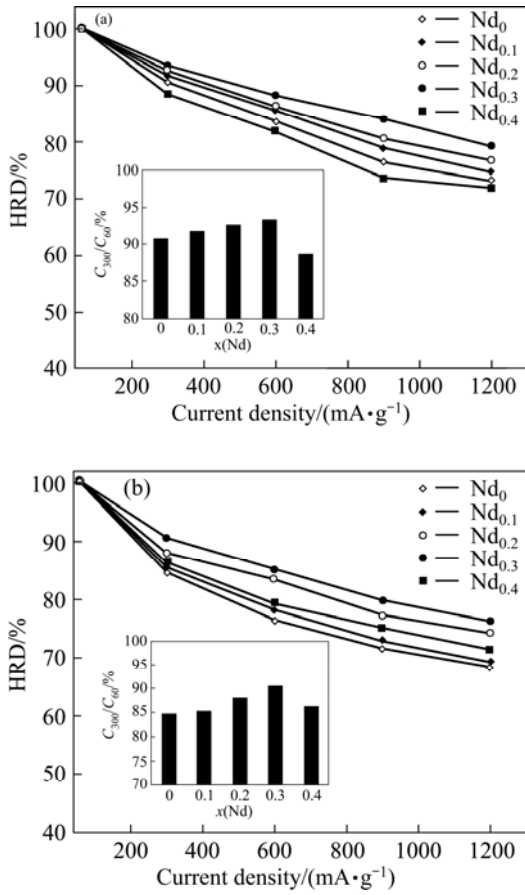


Fig. 7 Evolution of high rate discharge ability (HRD) of alloys with discharge current density: (a) As-cast; (b) As-annealed

$$\lg J = \lg \left(\pm \frac{6FD}{da^2} (C_0 - C_s) \right) - \frac{\pi^2}{2.303} \frac{D}{a^2} t \quad (1)$$

$$D = - \frac{2.303a^2}{\pi^2} \frac{d \lg J}{dt} \quad (2)$$

where J is the diffusion current density; F is the Faraday constant; D is the hydrogen diffusion coefficient; C_0 is the initial hydrogen concentration in the bulk of the alloy; C_s is the hydrogen concentration on the surface of the alloy particles; a is the alloy particle radius; d is the density of the hydrogen storage alloy; t is the discharge time. In Eq. (2), $d \lg J / dt$ is the slope of the linear region in Fig. 8. The D values calculated by Eq. (2) are also illustrated in Fig. 8. It is found that the D values of the as-cast and annealed alloys first grow and then decline with increasing Nd content. The Nd content corresponding to the maximum D values of the as-cast and annealed alloys is uniform with that corresponding to the largest HRD values of the as-cast and annealed alloys, suggesting that the hydrogen diffusion ability is a crucial factor of the electrochemical kinetics of the alloys.

Figure 9 shows the Tafel polarization curves of the as-cast and annealed alloy electrodes. It is evident that

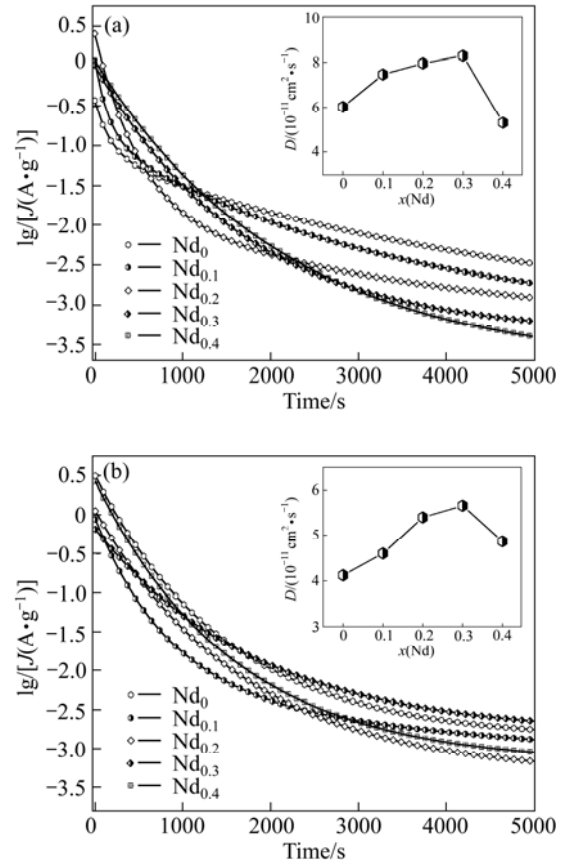


Fig. 8 Semilogarithmic curves of anodic current vs time responses of alloys: (a) As-cast; (b) As-annealed

each curve comprises an anode polarization process and a cathode polarization process. In all cases, the anodic current density grows to a limiting value and then falls. The current density at the inflection point is known as limiting current density (J_L), which indicates that an oxidation reaction takes place on the surface of the alloy electrode, and the generated oxidation product resists further penetration of hydrogen atoms [22]. The decrease of the anodic charge current density on cycling predicates that charging becomes more difficult. Hence, the limiting current density, J_L , may be regarded as a critical passivation current density, mainly dominated by the hydrogen diffusion in the bulk of the alloy during anodic polarization [23]. The J_L values of the as-cast and annealed alloys as a function of the amount of Nd substitution are demonstrated in Fig. 9. It is viewable that the J_L values of the as-cast and annealed alloys first increase then decrease with rising Nd content.

Figure 10 shows the electrochemical impedance spectra (EIS) of the as-cast and annealed alloy electrodes, which qualitatively reflects the charge-transfer ability on the surface of the alloy electrode. It is found that each EIS spectrum comprises two semicircles corresponding to two different frequency regions. As elucidated by KURIYAMA et al [24], the smaller semicircle in the

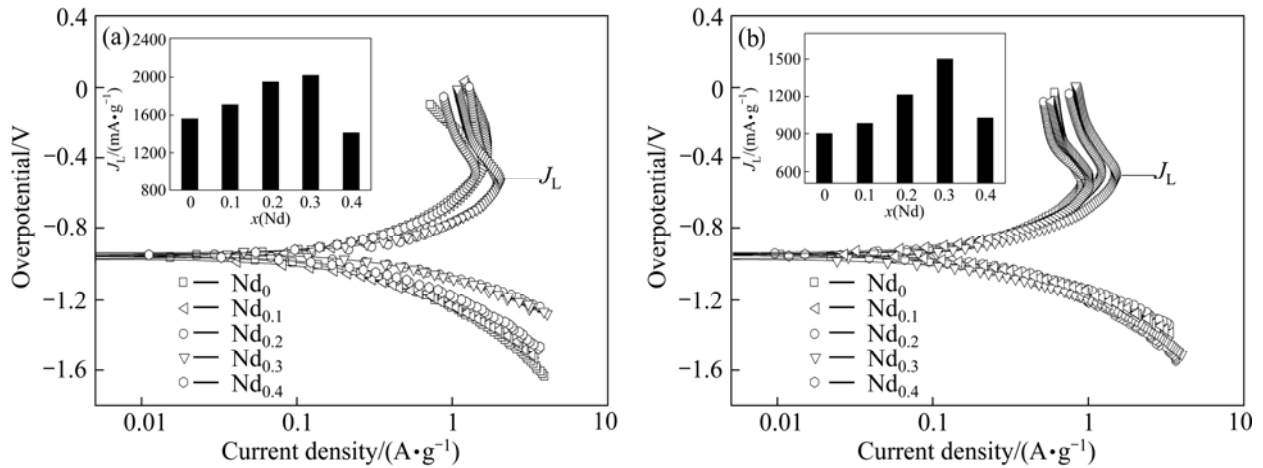


Fig. 9 Tafel polarization curves of as-cast and annealed alloy electrodes: (a) As-cast; (b) As-annealed

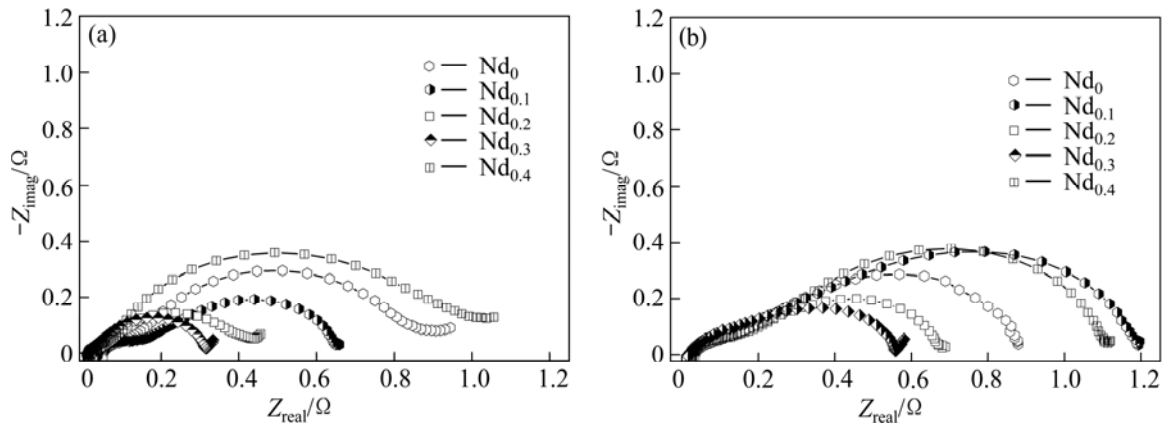


Fig. 10 Electrochemical impedance spectra (EIS) of alloy electrodes: (a) As-cast; (b) As-annealed

high frequency region corresponds to the contact resistance between the alloy powder and the conductive material, while the larger semicircle in the low frequency region equals the charge-transfer resistance on the alloy surface. Hence, the larger the radius of the semicircle in the low frequency region is, the larger the charge-transfer resistance of the alloy electrode will be. It is viewable from Fig. 10 that the radii of the large semicircles of the as-cast and annealed alloys in the low frequency first shrink and then expand with Nd content growing.

The above-mentioned results reveal that the HRD and the electrochemical kinetics of the as-cast and annealed alloys first grow and then decline with Nd content rising, which is ascribed to the change of the structure of the alloys resulting from substituting La with Nd. On one hand, the increased LaNi_5 phase by Nd substitution markedly improves the electrocatalytic activity of the alloy electrodes. On the other hand, upon the refined microstructure by Nd substitution, a lot of new crystallites and grain boundaries evolve, which may act as fast diffusion paths for hydrogen absorption [25], intensifying the HRD and electrochemical kinetics of the

alloy. However, it must be mentioned that the refined grains resulting from Nd substitution severely impair the charge-transfer rate on the alloy surface due to the fact that the refined grains effectively prohibit the pulverization of the alloy particles, and a lower new surface of the alloy electrode forms, decreasing the rate of charge transfer at the alloy-electrolyte interface. It is above-mentioned contrary impacts engendered by Nd substitution that yield a maximum HRD value of the alloy. The decreased HRD of the alloys by annealing is ascribed to the change of the structure produced by the annealing. The annealing treatment eliminates the casting internal strain and diminishes crystalline defects such as dislocations and grain boundaries, which not only increases the charge-transfer resistance of the alloy electrodes but also hinders the hydrogen diffusion from inner of the bulk to the surface, and subsequently brings on a drop in the electrochemical kinetic property.

4 Conclusions

1) The as-cast and annealed alloys comprise two major phases, $(\text{La,Mg})_2\text{Ni}_7$ and LaNi_5 . The substitution

of Nd for La brings on a decrease of $(\text{La}, \text{Mg})_2\text{Ni}_7$ phase and an increase of LaNi_5 phase in the alloys without changing the structures of the major phases of the alloys. Such substitution results in an evident refinement of the grains of the alloys.

2) The discharge capacities of the as-cast and annealed alloys first mount up and then fall with Nd content increasing, whereas their electrochemical cycle stabilities always grow with Nd content rising.

3) The annealing treatment remarkably enhances the discharge capacity and cycle stability of the alloys, whereas it slightly impairs the electrochemical kinetic property of the alloys.

References

- [1] KADIR K, SAKAI T, UEHARA I. RMg_2Ni_6 (R=La, Ce, Pr, Nd, Sm and Gd) built from MgNi_2 Laves-type layers alternating with AB_5 layers [J]. *J Alloys Compd*, 1997, 257: 115–121.
- [2] KOHNO T, YOSHIDA H, KAWASHIMA F, INABA T, SAKAI I, YAMAMOTO M, KANDA M. Hydrogen storage properties of new ternary system alloys: La_2MgNi_9 , $\text{La}_5\text{Mg}_2\text{Ni}_{23}$, $\text{La}_3\text{MgNi}_{14}$ [J]. *J Alloys Compd*, 2000, 311: L5–L7.
- [3] PAN H G, LIU Y F, GAO M X, LEI Y Q, WANG Q D. A Study of the structural and electrochemical properties of $\text{La}_{0.7}\text{Mg}_{0.3}(\text{Ni}_{0.85}\text{Co}_{0.15})_x$ ($x=2.5\text{--}5.0$) hydrogen storage alloys [J]. *J Electrochem Soc A*, 2003, 150: 565–570.
- [4] PAN H G, LIU Y F, GAO M X, ZHU Y F, LEI Y Q, WANG Q D. An investigation on the structural and electrochemical properties of $\text{La}_{0.7}\text{Mg}_{0.3}(\text{Ni}_{0.85}\text{Co}_{0.15})_x$ ($x=3.15\text{--}3.80$) hydrogen storage electrode alloys [J]. *J Alloys Compd*, 2003, 351: 228–234.
- [5] LIU Y F, PAN H G, GAO M X, ZHU Y F, LEI Y Q. Hydrogen storage and electrochemical properties of the $\text{La}_{0.7}\text{Mg}_{0.3}\text{Ni}_{3.825-x}\text{Co}_{0.675}\text{Mn}_x$ hydrogen storage electrode alloys [J]. *J Alloys Compd*, 2004, 365: 246–252.
- [6] LIU Y F, CAO Y H, HUANG L, GAO M X, PAN H G. Rare earth–Mg–Ni-based hydrogen storage alloys as negative electrode materials for Ni/MH batteries [J]. *J Alloys Compd*, 2011, 509: 675–686.
- [7] LIU Y F, PAN H G, YUE Y J, WU X F, CHEN N, LEI Y Q. Cycling durability and degradation behavior of La–Mg–Ni–Co-type metal hydride electrodes [J]. *J Alloys Compd*, 2005, 395: 291–299.
- [8] ZHANG Y H, LI B W, REN H P, GUO S H, QI Y, WANG X L. Structures and electrochemical cycle stability of $\text{La}_{0.75-x}\text{Pr}_x\text{Mg}_{0.25}\text{Ni}_{3.2}\text{Co}_{0.2}\text{Al}_{0.1}$ ($x=0\text{--}0.4$) alloys prepared by melt spinning [J]. *Mater Chem Phys*, 2009, 118: 129–134.
- [9] LIU Y F, PAN H G, GAO M X, LI R, LEI Y Q. Effect of Co content on the structural and electrochemical properties of the $\text{La}_{0.7}\text{Mg}_{0.3}\text{Ni}_{3.4-x}\text{Mn}_{0.1}\text{Co}_x$ hydride alloys II. Electrochemical properties [J]. *J Alloys Compd*, 2004, 376: 304–313.
- [10] ZHANG Y H, LI B W, REN H P, CAI Y, DONG X P, WANG X L. Cycle stabilities of the $\text{La}_{0.7}\text{Mg}_{0.3}\text{Ni}_{2.55-x}\text{Co}_{0.45}\text{M}_x$ (M=Fe, Mn, Al; $x=0, 0.1$) electrode alloys prepared by casting and rapid quenching [J]. *J Alloys Compd*, 2008, 458: 340–345.
- [11] ZHANG Y H, LI B W, REN H P, WU Z W, DONG X P, WANG X L. Investigation on structures and electrochemical characteristics of the as-cast and quenched $\text{La}_{0.5}\text{Ce}_{0.2}\text{Mg}_{0.3}\text{Co}_{0.4}\text{Ni}_{2.6-x}\text{Mn}_x$ ($x=0\text{--}0.4$) electrode alloys [J]. *J Alloys Compd*, 2008, 461: 591–597.
- [12] BANCZEK E P, ZARPELON L M C, FARIA R N, COSTA I. Corrosion resistance and microstructure characterization of rare-earth-transition metal–aluminum–magnesium alloys [J]. *J Alloys Compd*, 2009, 479: 342–347.
- [13] SHEN X Q, CHEN Y G, TAO M D, WU C L, DENG G, KANG Z Z. The structure and 233K electrochemical properties of $\text{La}_{0.8-x}\text{Nd}_x\text{Mg}_{0.2}\text{Ni}_{3.1}\text{Co}_{0.25}\text{Al}_{0.15}$ ($x=0.0\text{--}0.4$) hydrogen storage alloys [J]. *Int J Hydrogen Energy*, 2009, 34: 2661–2669.
- [14] SHEN X Q, CHEN Y G, TAO M D, WU C L, DENG G, KANG Z Z. The structure and high-temperature (333 K) electrochemical performance of $\text{La}_{0.8-x}\text{Ce}_x\text{Mg}_{0.2}\text{Ni}_{3.5}$ ($x=0.00\text{--}0.20$) hydrogen storage alloys [J]. *Int J Hydrogen Energy*, 2009, 34: 3395–3403.
- [15] PAN H G, CHEN N, GAO M X, LI R, LEI Y Q, WANG Q D. Effects of annealing temperature on structure and the electrochemical properties of $\text{La}_{0.7}\text{Mg}_{0.3}\text{Ni}_{2.45}\text{Co}_{0.75}\text{Mn}_{0.1}\text{Al}_{0.2}$ hydrogen storage alloy [J]. *J Alloys Compd*, 2005, 397: 306–312.
- [16] SONG Chun-hong. Investigation on effects of si to the phase structure and electrochemical performances of La–Mg–Ni system A_2B_7 type hydrogen storage alloys [D]. Baotou: School of Material and Metallurgy, Inner Mongolia University of Science and Technology, 2011. (in Chinese)
- [17] LÜ Ke. Effects of additive si and annealing technology on hydrogen storage performance of La–Mg–Ni system alloys [D]. Baotou: School of Material and Metallurgy, Inner Mongolia University of Science and Technology, 2011. (in Chinese)
- [18] PAN H G, JIN Q W, GAO M X, LIU Y F, LI R, LEI Y Q. Effect of the cerium content on the structural and electrochemical properties of the $\text{La}_{0.7-x}\text{Ce}_x\text{Mg}_{0.3}\text{Ni}_{2.875}\text{Mn}_{0.1}\text{Co}_{0.525}$ ($x=0\text{--}0.5$) hydrogen storage alloys [J]. *J Alloys Compd*, 2004, 373: 237–245.
- [19] ORIMO S, FUJII H. Materials science of Mg–Ni-based new hydrides [J]. *Appl Phys A*, 2001, 72: 167–186.
- [20] LIU Y F, PAN H G, GAO M X, ZHU Y F, GE H W, LI S Q, LEI Y Q. Investigation on the structure and electrochemical properties of the rare-earth Mg-based hydrogen storage electrode alloys [J]. *Acta Metall Sinica*, 2003, 39: 666–672.
- [21] ZHENG G, POPOV B N, WHITE R E. Electrochemical determination of the diffusion coefficient of hydrogen through an $\text{LaNi}_{4.25}\text{Al}_{0.75}$ electrode in alkaline aqueous solution [J]. *J Electrochem Soc*, 1995, 142: 2695–2698.
- [22] ZHAO X Y, DING Y, MA L Q, WANG L Y, YANG M, SHEN X D. Electrochemical properties of $\text{MmNi}_{3.8}\text{Co}_{0.75}\text{Mn}_{0.4}\text{Al}_{0.2}$ hydrogen storage alloy modified with nanocrystalline nickel [J]. *Int J Hydrogen Energy*, 2008, 33: 6727–6733.
- [23] RATNAKUMAR B V, WITHAM C, BOWMAN R C Jr, HIGHTOWER A, FULTZ B. Electrochemical studies on $\text{LaNi}_{5-x}\text{Sn}_x$ metal hydride alloys [J]. *J Electrochem Soc*, 1996, 143: 2578–2584.
- [24] KURIYAMA N, SAKAI T, MIYAMURA H, UEHARA I, ISHIKAWA H, IWASAKI T. Electrochemical impedance and deterioration behavior of metal hydride electrodes [J]. *J Alloys Compd*, 1993, 202: 183–197.
- [25] WU Y, HANA W, ZHOU S X, LOTOTSKY M V, SOLBERG J K, YARTYS V A. Microstructure and hydrogenation behavior of ball-milled and melt-spun Mg–10Ni–2Mm alloys [J]. *J Alloys Compd*, 2008, 466: 176–181.

铸态及退火态 $\text{La}_{0.8-x}\text{Nd}_x\text{Mg}_{0.2}\text{Ni}_{3.15}\text{Co}_{0.2}\text{Al}_{0.1}\text{Si}_{0.05}$ ($x=0\sim 0.4$) 合金的电化学贮氢性能

张羊换^{1,2}, 侯忠辉², 李保卫², 任慧平², 蔡颖², 赵栋梁¹

1. 钢铁研究总院 功能材料研究所, 北京 100081;
2. 内蒙古科技大学 国家重点实验室培育基地, 包头 014010

摘要: 通过铸造及退火处理制备 La-Mg-Ni 基 A_2B_7 型 $\text{La}_{0.8-x}\text{Nd}_x\text{Mg}_{0.2}\text{Ni}_{3.15}\text{Co}_{0.2}\text{Al}_{0.15}$ ($x=0, 0.1, 0.2, 0.3, 0.4$) 电极合金, 并研究 Nd 部分替代 La 对合金结构及电化学性能的影响。结果表明, 所有合金样品的主相均为六方结构的 Ce_2Ni_7 型 $(\text{La}, \text{Mg})_2\text{Ni}_7$ 及六方结构的 CaCu_5 型 LaNi_5 , 同时还有部分 LaNi_3 和 NdNi_5 残余相。铸态及退火态合金的放电容量及高倍率放电性能随着 Nd 含量的增加先增加后减小。当 $x=0.3$ 时, 铸态及退火态合金的放电容量达到最大值, 分别为 $380.3 \text{ mA}\cdot\text{h/g}$ 和 $384.3 \text{ mA}\cdot\text{h/g}$ 。合金的电化学循环稳定性随着 Nd 含量的增加而持续增加。当 Nd 含量从 0 增加至 0.4% 时, 铸态合金在第 100 次充放电循环时的容量保持率(S_{100})从 64.98% 增加至 85.17%, 而退火态合金的 S_{100} 值从 76.60% 增加至 96.84%。

关键词: 镍氢电池; 存氢; A_2B_7 型电极合金; 钕; 镧; 替代; 电化学性能

(Edited by Hua YANG)